# ARTICLES

## Comparative Study of $ABO_3$ Perovskite Compounds. 1. $ATiO_3$ (A = Ca, Sr, Ba, and Pb) Perovskites

**Zhao-Xu Chen, Yi Chen, and Yuan-Sheng Jiang***

*Lab of Mesostructured Materials Chemistry and Department of Chemistry, Nanjing University, Nanjing 210093, P. R. China*

*Received: August 27, 2001; In Final Form: February 25, 2002*

Comparative studies on the four $ATiO_3$ compounds are carried out to investigate the different ferroelectric behaviors of $ATiO_3$ on the basis of the experimental and theoretically optimized lattice structures. The stability predicted from the calculated total energies is in agreement with experimental observation. The obtained potential energy surfaces (PESs) show Ti displacements in $CaTiO_3$ and $SrTiO_3$ result in single-well potential whereas in $BaTiO_3$ and $PbTiO_3$ they produce double-well potential. In contrast to alkaline earth metal atoms, the PES of Pb displacement is double well. The calculated PES supports the experimental conclusion that Ti displaces from ⟨111⟩ in tetragonal structure. In addition, the calculated hopping barriers are in agreement with the prediction of the vibronic theory. Charge distribution and the Ti−O and A−O bonding situation are analyzed on the basis of electronic structure calculations. It is shown that symmetry lowering enhances Ti−O covalent bonding in all the titled compounds and A−O bonds have some degree of covalency, with Pb−O being the strongest. Analyses show that there is a relationship between the charges on A and A−O interactions and the ferroelectric behaviors of the $ATiO_3$ perovskite compounds.

### 1. Introduction

Ferroelectrics have wide applications in pyroelectronic detectors, imaging devices, optical memories, modulators, and deflectors.[1] An important group of ferroelectrics is that known as perovskite ferroelectrics.[1] The perfect perovskite structure is a cubic one with general formula $ABO_3$, where A is a divalent or monovalent metal and B is a tetra- or pentavalent atom. In the cubic structure, the A atoms are at the cube corners, B atoms at the body centers, and the oxygens at the face centers. Titanates, $ATiO_3$, where A = Ca, Sr, Ba, and Pb, exhibit different ferroelectric behaviors. It is known that $CaTiO_3$ and $SrTiO_3$ are incipient ferroelectrics,[1,2] whereas $BaTiO_3$ and $PbTiO_3$ are ferroelectrics having three (tetragonal, orthorhombic, and rhombohedral) and one (tetragonal) ferroelectric phases, respectively.[1] The ferroelectric phase transitions of $BaTiO_3$, especially that of $PbTiO_3$, were long considered as displacive type. In the displacive model[3] some or all of the constituent atoms are displaced from sites of point centrosymmetry in low-temperature phases. These displacements driven by softening of the appropriate phonon modes are of the same symmetry as the macroscopic order parameter. Although the displacive model has qualitatively explained many of the macroscopic and thermodynamic properties of $BaTiO_3$, there are quantitative discrepancies and a number of measurements in the literature that are not well explained by a displacive model.[4] On the other hand, the vibronic theory[5,6] deems the origin of ferroelectricity in $BaTiO_3$ to the vibronic mixing of the ground electronic state of the high-symmetry reference configuration with the excited states by low-symmetry nuclear displacement and the ferroelectric phase transitions are order−disorder type. In order−disorder model,[5−8] the rhombohedral phase is well-ordered. However, in the orthorhombic phase, the crystallographic cells form ordered chains 50−100 Å long parallel to the ⟨010⟩ direction, with each Ti displacement along two of the ⟨111⟩ axes. In the tetragonal phase, these chains form in two directions. Finally, in the cubic phase, chains form in all three cube-edge directions. Recently, more and more experiments, such as X-ray absorption fine structure (XAFS),[4,9−11] impulsive stimulated Raman scattering (IRIS),[12,13] electron paramagnetic resonance (EPR),[14] inelastic light scattering,[15] and neutron scattering,[16] have shown that the phase transitions of $BaTiO_3$ and $PbTiO_3$ are more order−disorder behavior. The ground-state structures of $BaTiO_3$ and $PbTiO_3$ are rhombohedral and tetragonal structures, respectively. The local structure of cubic, tetragonal, and orthorhombic $BaTiO_3$ is rhombohedral. For $PbTiO_3$ the local structure of cubic phase is tetragonal. In other words, the local distortions exist even in cubic $BaTiO_3$ and $PbTiO_3$. On the other hand, $SrTiO_3$, which has a structure very similar to that of $BaTiO_3$, has no local distortion.[17]

Semiempirical MO calculations on a series of $ATiO_3$ (A = Ca, Sr, and Ba) perovskites show that the bare force constant for $BaTiO_3$ is smaller than the ones for $CaTiO_3$ and $SrTiO_3$.[18] To explore different ferroelectric behaviors of $ATiO_3$ compounds, discrete variational Xα method (DV-Xα) calculation on $A_8TiO_6^{8+}$ (A = Ca, Sr, Ba, and Pb)[19] and full potential linearized augmented plane wave (LAPW) studies on $BaTiO_3$ and $PbTiO_3$[20−21] have also been performed. It is found that Ba is completely ionic and the difference between $BaTiO_3$ and $PbTiO_3$ is due to the significant A−O hybridization (covalent bonding) that exists in $PbTiO_3$ and does not occur in $BaTiO_3$.

10.1021/jp013301j CCC: $22.00 
Published on Web 09/05/2002

**TABLE 1: Lattice Parameters and Atomic Positions for Cubic, Tetragonal, and Rhombohedral Structures of $ATiO_3$ Compounds[a]**

| compounds | C | T | R |
|---|---|---|---|
| $CaTiO_3$ | $a = 3.892$(*3.897*) | $a = 3.837$, $c = 4.140$ | $a = 3.912$,$\alpha = 89.46°$ |
| | Ca(0,0,0) | Ca(*0,0, 0.070*) | Ca(*−0.011,−0.011,−0.011*) |
| | Ti(0.5,0.5,0.5) | Ti(*0.5,0.5, 0.525*) | Ti(*0.504,0.504,0.504*) |
| | O1(0.5,0.5,0) | O1(*0.5,0.5−0.032*) | O1(*0.538,0.538,0.024*) |
| | O2(0,0.5,0.5) | O2(*0,0.5, 0.446*) | O2(*0.024,0.538,0.538*) |
| | O3(0.5,0,0.5) | O3(*0.5,0, 0.446*) | O3(*0.538,0.024,0.538*) |
| $SrTiO_3$ | $a = 3.905$ (*3.922*) | $a = 3.889$, $c = 4.058$ | $a = 3.936$,$\alpha = 89.75°$ |
| | Sr(0,0,0) | Sr(*0,0, 0.045*) | Sr(*0.000,0.000,0.000*) |
| | Ti(0.5,0.5,0.5) | Ti(*0.5,0.5, 0.530*) | Ti(*0.505,0.505,0.505*) |
| | O1(0.5,0.5,0) | O1(*0.5,0.5, −0.015*) | O1(*0.534,0.534,0.025*) |
| | O2(0,0.5,0.5) | O2(*0,0.5, 0.469*) | O2(*0.025,0.534,0.534*) |
| | O3(0.5,0,0.5) | O3(*0.5,0, 0.469*) | O3(*0.534,0.025,0.534*) |
| $BaTiO_3$ | $a = 3.996$(*3.990*) | $a = 3.992$, $c = 4.036$ | $a = 4.001$,$\alpha = 89.87°$ |
| | Ba(0,0,0) | Ba(0, 0, 0) | Ba(0.013, 0.013, 0.013) |
| | Ti(0.5,0.5,0.5) | Ti(0.5,0.5, 0.5135) | Ti(0.5,0.5,0.5) |
| | O1(0.5,0.5,0) | O1(0.5,0.5,−0.025) | O1(0.531,0.524,0.031) |
| | O2(0,0.5,0.5) | O2(0,0.5, 0.485) | O2(0.031,0.524,0.524) |
| | O3(0.5,0,0.5) | O3(0.5,0, 0.485) | O3(0.531,0.031,0.524) |
| $PbTiO_3$ | $a = 3.968$(*3.928*) | $a = 3.904$, $c = 4.152$ | $a = 3.981$,$\alpha = 89.11°$ |
| | Pb(0,0,0) | Pb(0,0,0) | Pb(*−0.052,−0.052,−0.052*) |
| | Ti(0.5,0.5,0.5) | Ti(0.5,0.5, 0.540) | Ti(*0.502,0.502,0.502*) |
| | O1(0.5,0.5,0) | O1(0.5,0.5, 0.112) | O1(*0.562,0.562,0.034*) |
| | O2(0,0.5,0.5) | O2(0,0.5, 0.612) | O2(*0.034,0.562,0.562*) |
| | O3(0.5,0,0.5) | O3(0.5,0, 0.612) | O3(*0.562,0.034,0.562*) |

[a] The experimental cubic lattice parameter of $CaTiO_3$ is taken from ref 24. $SrTiO_3$, $BaTiO_3$, and $PbTiO_3$ cubic lattice parameters are from ref 23. Italic values are theoretically optimized results. C, T, and R denote the cubic (*Pm*3*m*), tetragonal (*P*4*mm*), and rhombohedral (*R*3*m*) structures, respectively.

According to this conclusion it seems that stronger covalency of A−O bonds would correspond to larger ferroelectricity. This point of view is questionable if one considers $CaTiO_3$ and $SrTiO_3$ that have more covalent A−O bonds than $BaTiO_3$ do not exhibit ferroelectricity. At this stage one may ask: how does one predict the ferroelectricity of perovskites? Or equivalently, is there any criterion by which we can predict whether a perovskite compound possesses ferroelectricity or not? Obviously, studies trying to the answer this question are of significance, especially for materialists.

To obtain a thorough and complete understanding of the ferroelectric phenomenon of perovskite ferroelectrics, in this paper we perform a comparative study on $CaTiO_3$, $SrTiO_3$, $BaTiO_3$, and $PbTiO_3$ with periodic density functional theory (DFT) methods. Considering that most of the previous investigations on ferroelectricity of perovskites are focused on the role of B and B−O interactions, and fewer are concerned with the role of A and A−O on ferroelectricity, we will pay special attention to A-site atoms and their interaction with oxygen atoms. The arrangement of the present paper is as follows. In section 2 the calculation details are presented. Results of lattice optimizations for three kinds of crystal structures of four $ATiO_3$ compounds are displayed in section 3.1. Potential energy surfaces (PESs) of Ti and A-site atomic displacements as well as the PES of Ti hopping between different sites in $BaTiO_3$ are discussed in section 3.2. Electronic structures including charge distribution, bond orders, and overlap populations for various structures are analyzed in sections 3.3−3.5, respectively. Finally, conclusions are given.

## 2. Calculation Details

One of the goals of this paper is to search for the character of electronic structure of perovskite ferroelectrics. We will confine our studies to cubic (*Pm*3*m*), tetragonal (*P*4*mm*), and rhombohedral (*R*3*m*) structures because, according to Curie law, the ferroelectric tetragonal and rhombohedral structures derived from paraelectric *Pm*3*m* group must belong to *P*4*mm* and *R*3*m* structures, respectively.[22] As pointed out in the Introduction, the local structures of cubic and tetragonal $BaTiO_3$ are still rhombohedral structure and the cubic $PbTiO_3$ has tetragonal local structure. For $CaTiO_3$ and $SrTiO_3$ neither *P*4*mm* (tetragonal) nor *R*3*m* (rhombohedral) structure has been observed. Their tetragonal phase space group belongs to *I*4/*mcm*.[23,24] That is to say, most structures we will investigate do not exist in reality. However, as a theoretical approach, we think it is still reasonable to perform studies on the structures that exist only in theory. By comparing the calculated results, one gets a better understanding why these structures are hard to exist.

With the above in mind, we first optimized the lattice parameters and atomic positions for those *P*4*mm* and *R*3*m* structures whose experimental crystallographic structures are not available. The optimizations are performed with pseudopotential methods[25] using CASTEP code[26] in the framework of generalized gradient approximation (GGA).[27] To test the reliability of the calculation conditions, we have also optimized the unit cell parameters of cubic phases for all four kinds of compounds. The maximum error is ∼1%, indicating that agreement with experimental results is satisfactory. LCAO calculations on all the structures (see Table 1) are performed with the DSolid program, a newly developed version of DMol.[28,29] Due to the smaller frontier orbital gap, the calculations of the cubic structure cannot converge unless charge smearing among all orbitals in the range of 0.02 au of the Fermi level is allowed. To keep consistency, computations on the other structures are carried out at the same calculation condition. For the details of pseudopotential total energy and LCAO calculations, we refer readers to refs 30 and 31.

## 3. Results and Discussion

**3.1. Lattice Parameters, Atomic Positions, and Total Energies.** Table 1 lists the lattice parameters and atomic fractional coordinates for each structure studied in this paper. It is noticeable from Table 1 that the theoretical lattice parameters (values in the parentheses) for the four cubic

**TABLE 2: Calculated Total Energies (eV)**

| compounds | C | T | R |
|---|---|---|---|
| $CaTiO_3$ | −2395.2667967 | −2395.1847610 | −2395.1586218 |
| $SrTiO_3$ | −2231.1946326 | −2231.0862867 | −2231.0771528 |
| $BaTiO_3$ | −2098.5813441 | −2098.5889071 | −2098.6159956 |
| $PbTiO_3$ | −2965.6913685 | −2966.0333608 | −2965.9661175 |

structures are in good agreement with the corresponding experimental ones, implying that the theoretical results are reasonable. From Table 1 one can see that the lattice volume of $PbTiO_3$ is between that of $BaTiO_3$ and $SrTiO_3$ and the theoretical results well reproduce the trend that from $CaTiO_3$ to $BaTiO_3$ the lattice volumes increase. The data in Table 1 also show that with an increase of atomic number of alkaline earth metals the tetragonal lattice strain ($c/a$) and rhombohedral strain($\alpha$) decrease.

The calculated total energies are displayed in Table 2. It is observed from Table 2 that the most stable structures for $BaTiO_3$ and $PbTiO_3$ are *R*3*m* and *P*4*mm*, respectively, which is in agreement with experimental results stating that their ground-state structures are *R*3*m* and *P*4*mm*, respectively.[16] Among the three kinds of structures the *Pm*3*m* structures of both $CaTiO_3$ and $SrTiO_3$ are the lowest in total energies, in agreement with the fact that neither *P*4*mm* nor *R*3*m* is the ground-state structure of $CaTiO_3$ and $SrTiO_3$. In other words, it is hard for them to possess ferroelectric tetragonal and rhombohedral structures. In fact, as the temperature reduces, $CaTiO_3$ and $SrTiO_3$ transform from cubic into the tetragonal *I*4/*mcm* structures. The calculated total energies of *I*4/*mcm* $CaTiO_3$ per formula unit are lower by 0.0653 eV than the cubic's.

To verify the order−disorder model, we have also calculated the total energy for the orthorhombic structure of $BaTiO_3$ on the basis of Comes' eight-site model[7,8] using the superlattice technique. For the sake of simplification, the local rhombohedral structure is determined by scanning Ti displacement along the ⟨111⟩ direction while the barium and oxygen atoms remain fixed. The lattice parameters are $a = b = c = 4.00$ Å and $\alpha = 90.0°$. The calculated magnitude of displacement is close to the experimental result[4] (see section 3.2). The calculated total energy per formula for the order−disorder model (−2098.503104 eV) is lower than that of the corresponding average crystallographic structure (−2098.396689 eV), indicating that the eight-site model is more favorable energetically.

**3.2. Potential Energy Surface (PES).** The above total energy calculations show that the ground states of $BaTiO_3$ and $PbTiO_3$ are rhombohedral and tetragonal structures, respectively, whereas cubic structures of $CaTiO_3$ and $SrTiO_3$ are lower in energy than those of the corresponding tetragonal and rhombohedral structures. To shed light on the difference between the four $ATiO_3$ compounds, we present potential energy surfaces (PESs) of sublattice displacement of Ti and A-site metal atoms.

The potential energy surfaces of Ti displacement in $BaTiO_3$ and $PbTiO_3$ have been reported previously by Cohen and Krakauer.[20,21] They found that the potential well depth of rhombohedral displacement is deeper than the one of tetragonal displacement. In ref 30 potential energy surfaces of various sublattice displacements in $BaTiO_3$ and influence of strain and lattice parameter on them are reported and analyzed. It is shown that Ti displacement as well as Ti and O coupled displacement results in double-well potential and larger lattice parameter and strain lead to deeper well. Here we investigate the PES of Ti displacement along ⟨001⟩ and ⟨111⟩ and of A-site metal atoms along ⟨001⟩, respectively, in the four $ATiO_3$ compounds. To simplify the matter, influences of lattice strain and coupled atomic displacement are not examined. The unit cell parameters for $CaTiO_3$, $SrTiO_3$, $BaTiO_3$, and $PbTiO_3$ are 3.892, 3.905, 4.00, and 3.968 Å, respectively.

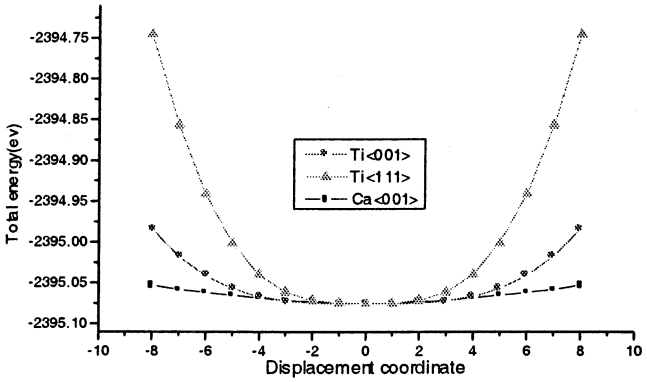


**Figure 1.** Potential energy surfaces of Ti and Ca ion displacement in $CaTiO_3$.

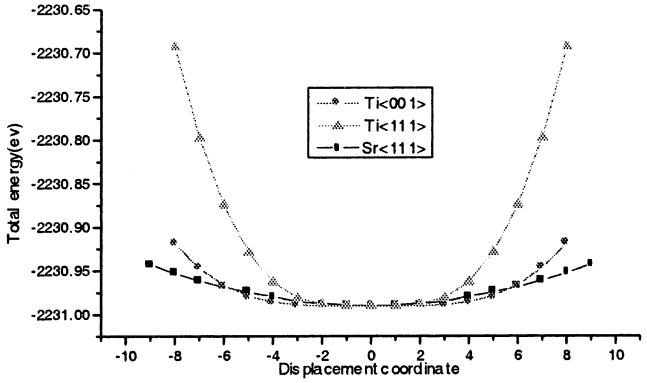


**Figure 2.** Potential energy surfaces of Ti and Sr displacement in $SrTiO_3$.

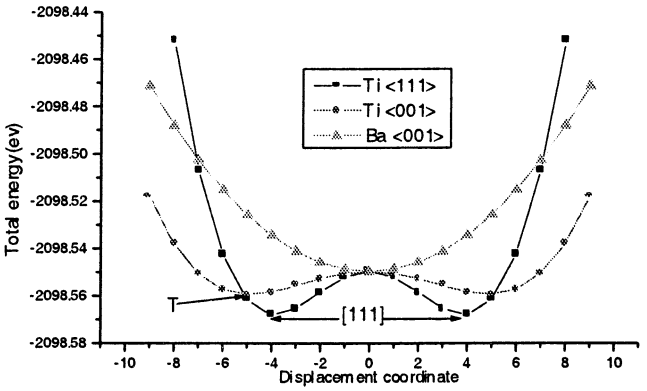


**Figure 3.** Potential energy surfaces of atomic displacement in $BaTiO_3$.

Figures 1−4 illustrate the calculated potential energy surfaces (PESs). The obtained PES clearly demonstrates the different behaviors between ferroelectrics ($BaTiO_3$ and $PbTiO_3$) and incipient ferroelectrics ($CaTiO_3$ and $SrTiO_3$). From Figures 1 and 2 we can see that the PESs of the Ti displacement in $CaTiO_3$ and $SrTiO_3$ are single-well potentials. On the contrary, in $BaTiO_3$ and $PbTiO_3$ Ti displacements result in double wells (see Figures 3 and 4), indicating that Ti displacements lower the total energies of $BaTiO_3$ and $PbTiO_3$. The theoretical minimum of the Ti shift along ⟨111⟩ in $BaTiO_3$ is ∼0.16 Å away from the center of the oxygen octahedron, in agreement with experimental results[4] (0.19 Å at 35 K and 0.16 Å at 750 K). It is worth noting that in $BaTiO_3$ the well depth of Ti displacement along ⟨111⟩ is deeper than that along ⟨001⟩ , which is in line with previous results.[20−21]

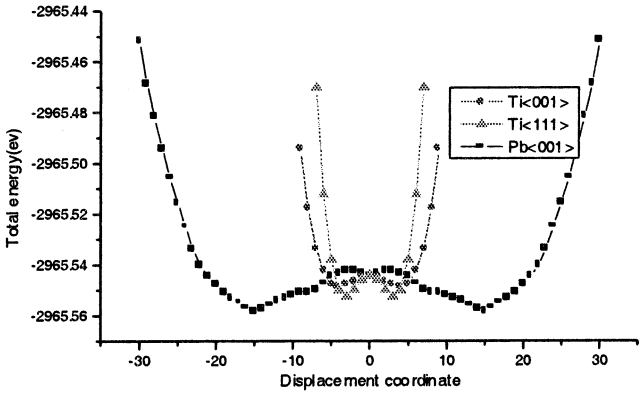


**Figure 4.** Potential energy surface of Ti and Pb displacement.

From Figures 1−3 one can also see that the potential energy surfaces of the three alkaline earth metal atom displacements along ⟨001⟩ are single well. Unlike those of alkaline earth metal atoms, the displacement PES of Pb is double-well potential,[32] which may, to a certain extent, explain why Pb displacements in $PbTiO_3$ are so large. It is noted from Figure 4 that the well depth (∼16 meV) of Pb displacement is much deeper than that of Ti displacement (∼4 meV), indicating that Pb plays a dominant role in the ferroelectric phase transition of $PbTiO_3$.

Examinations show that with Ti displacement the Mayer bond orders[33] of Ti−O bonds in all compounds have the same variation trend: they all increase as Ti atoms displace from the center of oxygen octahedron (of course, as Ti shifts, one of the longer Ti−O1 becomes weaker and the corresponding bond order decreases). On the other hand, A−O bond orders in different compounds exhibit different behaviors. The Ba−O bond order increases, whereas the bond orders of Ca−O and Sr−O tend to decrease. For $PbTiO_3$ the bond order of Pb−O1 decreases with Ti displacement; however, the Pb−O2 bond order increases. These results seem to indicate that different ferroelectric behaviors of $ATiO_3$ have something to do with the A−O interaction.

The vibronic theory[5,6] presents a vivid picture for ferroelectric phase transitions of $BaTiO_3$: The adiabatic potential in the titanium site has eight equivalent minima along the trigonal axes of the cubic environment. The three phase transitions are due to thermal averages that consequently involve two, four, and eight minima in orthorhombic, tetragonal, and cubic phases, respectively. However, the barrier heights are different. Therefore as temperature goes up, the lowest barrier (the orthorhombic saddle points) is overcome, resulting in orthorhombic phase. Then the barrier at the tetragonal saddle points is surmounted at higher temperatures, which leads to tetragonal polarization. Finally when the barrier between the two minima along the space diagonal of the cube is overcome, we obtain the cubic phase. According to ref 4, Ti atoms can hop between the various sites allowed by the order−disorder model in each phase. Obviously, knowledge about the energy barrier heights between the two minima along different directions is useful. With this in mind, we have calculated energy barriers of Ti hopping in $BaTiO_3$ from [111] to [$\bar{1}$11] and [1$\bar{1}$1] sites (see Figure 5) with strain ($a$ = 3.992 Å and $c$ = 4.0361 Å) and without strain ($c/a$ = 1 and $c$ = 4.00 Å), respectively. The positions of [111] in each structure are determined by scanning the potential energy surface of Ti displacement alone. Figures 6 and 7 display the energy barrier of Ti hopping in strained and unstrained structures, respectively. It can be seen from Figure 6 that the energy barrier of Ti hopping from [111] to [1$\bar{1}$1] is the lowest (∼2.6 meV). Due to symmetry, the hopping barrier from [111] to [$\bar{1}$11] is the same as that from [111] to [1$\bar{1}$1]. The barriers of hopping from [111] to [11$\bar{1}$] are the highest. From Figures 6 and 7 one can see that the barriers of Ti hopping between sites in the plane perpendicular to the polar axis (*Z* axis in Figure 5) are lower than the ones between sites parallel to the axis. It is interesting to notice from Figure 6 that our calculated hopping barriers are in good agreement with the prediction of the vibronic theory[5] that the barrier height between two neighboring minima is smallest along the edge of the cube and greater along the side diagonal. It is also noted that the magnitude of all the hopping barriers is not very high. In fact, the highest (from [111] to [11$\bar{1}$] is only 9.2 meV, indicating that it is easy for Ti to hop between various allowed sites, though in tetragonal structure the pathway from [111] to [1$\bar{1}$1] is the favorite one.

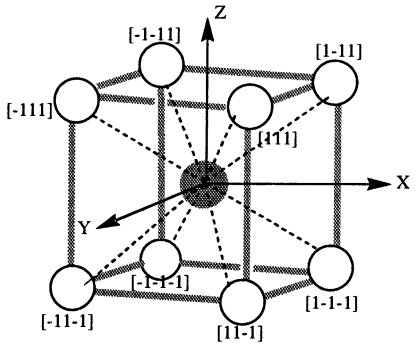


**Figure 5.** Illustration of eight site model.

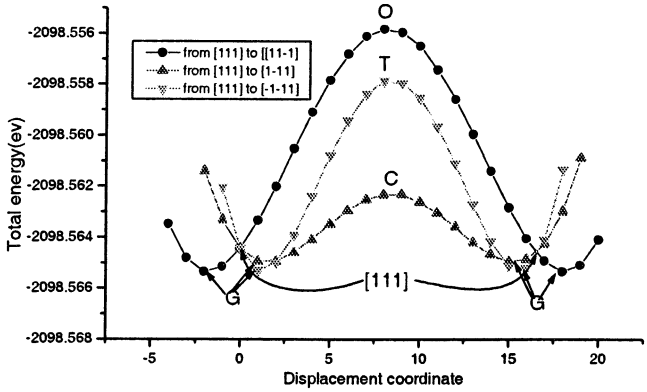


**Figure 6.** Hopping barrier of Ti atoms in strained structure.

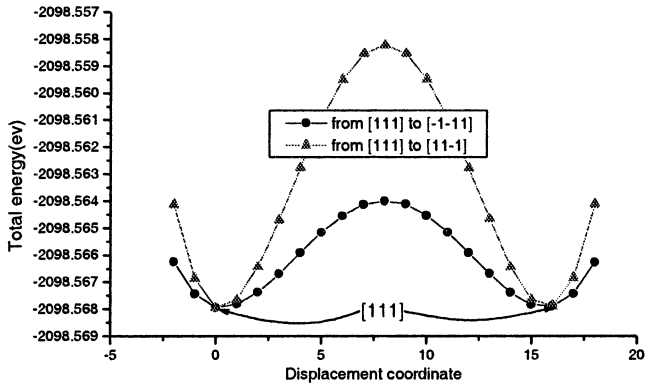


**Figure 7.** Hopping energy barrier of Ti atoms in unstrained structure.

The PES of Ti hopping brings some evidence supporting the order−disorder model. From Figure 3 one can see that there is a local minimum (point T in Figure 3) of Ti displacement along [001]. However, in Figure 6 one can see that point T is a maximum point along the pathway from [111] to [1$\bar{1}$1], indicating that point T is a saddle point. Points O and C that

**TABLE 3: Calculated Hirshfeld Charges**

| compounds | | A | Ti | O1 | O2 |
|---|---|---|---|---|---|
| $CaTiO_3$ | C | 0.7319 | 0.6070 | −0.4464 | −0.4464 |
| | T | 0.7227 | 0.5723 | −0.4353 | −0.4243 |
| | R | 0.7267 | 0.5853 | −0.4372 | −0.4372 |
| $SrTiO_3$ | C | 0.7046 | 0.6058 | −0.4374 | −0.4374 |
| | T | 0.7035 | 0.5830 | −0.4337 | −0.4190 |
| | R | 0.7041 | 0.5883 | −0.4308 | −0.4308 |
| $BaTiO_3$ | C | 0.6775 | 0.5979 | −0.4264 | −0.4264 |
| | T | 0.6798 | 0.5919 | −0.4305 | −0.4145 |
| | R | 0.6804 | 0.5844 | −0.4225 | −0.4225 |
| $PbTiO_3$ | C | 0.6855 | 0.5406 | −0.4092 | −0.4092 |
| | T | 0.7008 | 0.4936 | −0.4023 | −0.3898 |
| | R | 0.6522 | 0.4926 | −0.3815 | −0.3815 |

correspond approximately to Ti sites in average crystallographic structure are also saddle points.

The PES of Ti hopping in $BaTiO_3$ also reveals a hint supporting the experimental conclusion that Ti displaces away from ⟨111⟩ axes to the polar axis due to strain. Comparing Figures 6 and 7, one can see that in the unstrained structure the minimum is at [111]. In the strained structure, however, the minimum point is no longer at the [111] site, instead it deviates from [111] slightly to point G (see Figure 6), indicating that in the tetragonal structure the Ti ion displaces away from the ⟨111⟩ direction, which is qualitatively in agreement with the EXAFS measurements[4] showing that Ti displacement in the tetragonal phase are actually displaced from the ⟨111⟩ direction by 11.7(1.1)° toward the *c* axis.

**3.3. Atomic Charges.** In the above sections we have discussed the total energies and potential energy surfaces. Now we turn to analyze the electronic structures of different structures for the four kinds of $ATiO_3$ compounds. Although most of the structures do not exist in reality, comparison of these results would undoubtedly contribute to make a better understanding of the different ferroelectric behaviors in these perovskites. In the following sections, we will discuss the charge distribution, Mayer bond orders, and overlap populations calculated with DMol code[28,29] for three kinds of structures of four compounds.

The static atomic charge is not observable within the confines of quantum mechanics. Hence it is not possible to define it in a unique manner. As Mulliken charges are strongly basis set dependent, we adopt Hirshfeld charges[34] instead. Table 3 lists the calculated Hirshfeld charges. It is notable from the table that for the titanates of the three alkaline earth metal, as the atomic number of A increases the charge absolute values on A and O atoms tend to decrease. The behavior of Ti atomic charges seems a little complicated, though for the cubic structures they also decrease with increasing of A atomic number.

Comparing the calculated charges on A atoms in Table 3 and the corresponding total energies in Table 2, one can see that A-site atoms in structures with lower total energy tend to have larger positive charges. For example, Pb(0.7008*e*) in T and Ba-(0.6804*e*) in R are the greatest among the three corresponding structures of $PbTiO_3$ and $BaTiO_3$. So are Ca and Sr charges in the cubic structures. It is interesting to note that A-site atoms in R of $BaTiO_3$ and T of $PbTiO_3$ have the largest positive charges (both $BaTiO_3$ and $PbTiO_3$ are ferroelectrics) whereas the charges on Ca and Sr in T and R are smaller than the values of the corresponding cubic structures. It is also worth noting that Pb charges in R are lower than the ones in cubic $PbTiO_3$. These results seem to imply that the charges on A-site atoms are closely related to ferroelectricity of (pure) perovskite compounds.

**3.4. Bond Orders.** Mayer bond orders[33] are related to the exchange effects in bonding between the atoms and, they measure the degree of covalent bonding.[35,36] Though they are basis set dependent, their relative changes in a series of molecules of a similar structure can give us additional information and may help in understanding the structural features of the systems studied.[37] Table 4 contains the calculated Mayer bond orders.

**TABLE 4: Calculated Mayer Bond Orders[a]**

| compounds | | Ti−O1 | Ti−O2 | A−O1 | A−O2 |
|---|---|---|---|---|---|
| $CaTiO_3$ | C | 0.2551 | 0.2551 | 0.3963 | 0.3963 |
| | T | 0.9883 (0.1867) | 0.7559 | 0.3541 | 0.2653 |
| | R | 0.6800 (0.4179) | 0.6800 | 0.3721 | 0.3721 |
| $SrTiO_3$ | C | 0.3243 | 0.3243 | 0.3268 | 0.3268 |
| | T | 0.9538 (0.2327) | 0.6665 | 0.3254 | 0.2286 |
| | R | 0.7025 (0.3748) | 0.7025 | 0.3042 | 0.3042 |
| $BaTiO_3$ | C | 0.5276 | 0.5276 | 0.1174 | 0.1174 |
| | T | 0.9000 (0.3130) | 0.6421 | 0.1378 | 0.1274 |
| | R | 0.9147 (0.3920) | 0.9147 | 0.1305 | 0.1305 |
| $PbTiO_3$ | C | 0.5164 | 0.5164 | 0.5008 | 0.5008 |
| | T | 1.1873 (0.1662) | 0.9106 | 0.5251 | 0.4057 |
| | R | 1.1015 (0.3612) | 1.1015 | 0.4673 | 0.4673 |

[a] Values in parentheses are the bond orders for the longer Ti−O1 bonds.

Examining the data in Table 4, one can see with an increase of atomic number of the three alkaline earth metal atoms, the Ti−O bond orders of the cubic structure increase. The change trend of Ti−O bond order due to symmetry lowering is similar for the four $ATiO_3$ compounds. The Ti−O2 and shorter Ti−O1 bond orders in T (R) are much larger than the corresponding values in C, indicating that in lower symmetry structures Ti−O bonding is enhanced. Due to lengthened distances, the longer Ti−O1 bond orders (values in parentheses) are obviously smaller than the other Ti−O bond orders.

The calculated Mayer bond orders clearly show that A−O bonds, even the Ba−O bonds, have some extent of covalency, in agreement with the experiment[38] and band−band decomposition.[39,40] The obtained bond order sequence, Pb−O > Ca−O > Sr−O > Ba−O, is consistent with the notion that the smaller electronegativity gap between bonded atoms corresponds to more covalent bonding. Our calculated bond order of Pb−O is larger than that of Ba−O, indicating that Pb−O is more covalent than Ba−O, which is in agreement with ref 20. It is interesting to note that for the two incipient ferroelectrics, $CaTiO_3$ and $SrTiO_3$, the A−O1 bond orders in cubic phases are larger than those in the tetragonal and rhombohedral structures whereas for $BaTiO_3$ and $PbTiO_3$, the A−O1 orders in ferroelectric phases are larger than the ones of the corresponding cubic structures.

Our calculated bond orders do not conform to the idea that the presence of A−O covalency should enhance the Ti−O interaction.[41] As can be seen in Table 4, the Ca−O bond orders (0.3963) in C are larger than the corresponding bond orders (0.3721) in R. However, Ti−O bond orders (0.2551) in the cubic structure are smaller than the ones (0.6800 and 0.4179) in rhombohedral $CaTiO_3$. Comparison of Ti−O and A−O bond orders in different compounds also shows that the presence of A−O covalency does not enhance the Ti−O interaction. It is worth noting that for the two incipient ferroelectrics ($CaTiO_3$ and $SrTiO_3$) the A−O bond orders in the cubic structure are larger than those of Ti−O, whereas for two ferroelectrics ($BaTiO_3$ and $PbTiO_3$) their A−O orders are smaller than the ones of Ti−O.

**3.5. Overlap Populations.** Overlap populations reflect the electron accumulations in the bonding region. They can provide detailed information about chemical bonding. To obtain more knowledge about the Ti−O and A−O covalent bonding, we turn to analyze the overlap populations between atomic orbitals

**TABLE 5: Overlap Populations between A-Site Metal Atomic Orbitals and Oxygen Atomic Orbitals of Different Structures[a]**

| compounds | A−O1 | C | T | R | A−O2 | C | T | R |
|---|---|---|---|---|---|---|---|---|
| $CaTiO_3$ | 4s−2s | 227 | 125 | 195 | 4s−2s | 227 | 200 | 195 |
| $SrTiO_3$ | 5s−2s | 169 | 111 | 160 | 5s−2s | 169 | 181 | 160 |
| | $4p_y-2p_y$ | −22 | −22 | −32 | $4p_y-2p_y$ | −22 | −34 | −32 |
| | $4p_x-2p_x$ | −22 | −22 | −32 | $4p_z-2p_z$ | −22 | −34 | −32 |
| $BaTiO_3$ | 6s−2s | 78 | 83 | 91 | 6s−2s | 78 | 90 | 91 |
| | $5p_y-2p_y$ | −54 | −55 | −56 | $5p_y-2p_y$ | −54 | −57 | −56 |
| | $5p_z-2p_z$ | −11 | −10 | −10 | $5p_z-2p_z$ | −54 | −53 | −56 |
| | $5p_x-2p_x$ | −54 | −55 | −56 | $5p_x-2p_x$ | −10 | −10 | −9 |
| $PbTiO_3$ | 6s−2s | −87 | −107 | −121 | 6s−2s | −87 | −91 | −121 |
| | $6p_z-2s$ | | 15 | 16 | $6p_y-2s$ | | | 16 |
| | $6p_y-2p_y$ | 94 | 74 | 67 | $6p_y-2p_y$ | 94 | 74 | 67 |
| | $6p_z-2p_z$ | −25 | −10 | | $6p_z-2p_z$ | 94 | 104 | 67 |
| | $6p_x-2p_x$ | 94 | 74 | 67 | $6p_x-2p_x$ | −25 | | |

[a] All the overlap populations are multiplied by 1000, and values less than 10 are omitted.

**TABLE 6: Ti−O Overlap Populations of $CaTiO_3$[a]**

| Ti−O1 | C | T | R | Ti−O2 | C | T | R |
|---|---|---|---|---|---|---|---|
| 2s−4s | −206 | −87 | −177 | 2s−4s | −206 | −196 | −177 |
| $2p_y-4p_y$ | 67 | 51 | 57 | $2p_y-4p_y$ | 67 | 52 | 57 |
| $2p_z-4p_z$ | 34 | 39 | 44 | $2p_z-4p_z$ | 67 | 46 | 57 |
| $2p_x-4p_x$ | 67 | 51 | 57 | $2p_x-4p_x$ | 34 | 38 | 44 |
| $2p_z-3d_{yz}$ | | | 15 | $2p_x-3d_{xy}$ | | | 16 |
| $2p_y-3d_{yz}$ | | 35 | 8 | $2p_z-3d_{z^2}$ | | 30 | |
| $2p_z-3d_{z^2}$ | | 22 | | $2s-3d_{z^2}$ | 26 | 14 | 21 |
| $2s-3d_{z^2}$ | 105 | 66 | 82 | $2p_x-3d_{xz}$ | | 70 | 15 |
| $2p_z-3d_{xz}$ | | | 14 | $2s-3d_{x^2-y^2}$ | 79 | 56 | 62 |
| $2p_x-3d_{xz}$ | | 35 | | $2p_z-3d_{x^2-y^2}$ | | | 19 |

[a] See footnote for Table 5.

**TABLE 7: Ti−O Overlap Populations of $SrTiO_3$[a]**

| Ti−O1 | C | T | R | Ti−O2 | C | T | R |
|---|---|---|---|---|---|---|---|
| 2s−4s | −131 | −72 | −134 | 2s−4s | −131 | −166 | −134 |
| $2p_y-4p_y$ | 57 | 53 | 54 | $2p_y-4p_y$ | 57 | 49 | 54 |
| $2p_z-4p_z$ | 59 | 48 | 52 | $2p_z-4p_z$ | 57 | 50 | 54 |
| $2p_x-4p_x$ | 57 | 53 | 54 | $2p_x-4p_x$ | 59 | 55 | 52 |
| $2p_z-3d_{yz}$ | | | 18 | $2p_x-3d_{xy}$ | | | 12 |
| $2p_y-3d_{yz}$ | | 27 | | $2p_z-3d_{z^2}$ | | 19 | |
| $2p_z-3d_{z^2}$ | | 14 | | $2s-3d_{z^2}$ | 25 | 17 | 22 |
| $2s-3d_{z^2}$ | 103 | 79 | 87 | $2p_z-3d_{xz}$ | | | 12 |
| $2p_z-3d_{xz}$ | | | 18 | $2s-3d_{x^2-y^2}$ | 77 | 66 | 65 |
| $2p_x-3d_{xz}$ | | 27 | | $2p_z-3d_{x^2-y^2}$ | | 10 | |
| $2p_y-3d_{yz}$ | | | | $2p_y-3d_{yz}$ | | 46 | |

[a] See footnote for Table 5.

(AOs) of metal atoms and oxygen atoms. Table 5 lists the calculated overlap populations.

From Table 5 one can see that the three alkaline earth metal atoms bond to the oxygen 2s AO with their *n*s valence orbitals. With increasing A atomic number, the *n*s−2s bonding interaction decreases and the $(n-1)$p−2p antibonding increases, which leads to reduction of A−O bond orders (see Table 4). The data in Table 5 clearly show that the major difference between Pb−O and Ca(Sr and Ba)−O is that Pb bonds to O mainly through p−p bonding whereas the three alkaline earth metal atoms attach to oxygen atoms through their *n*s−2s interactions.

The overlap populations between titanium and oxygen atoms are displayed in Tables 6−9. Examining the data in the four tables one can see that the Ti−O bonding situations in the same structures of different compounds are similar. In C structure, there are three $\sigma$-type (2s−4s, $2p_z-4p_z$, and $2s-3d_{z^2}$) and two $\pi$-type ($2p_y-4p_y$ and $2p_x-4p_x$) bondings between O1 and the central Ti (2s−4s in the Ca, Sr, and Ba titanates are antibonding states). With increasing A atomic number the 2s−4s overlap

**TABLE 8: Ti−O Overlap Populations of $BaTiO_3$[a]**

| Ti−O1 | C | T | R | Ti−O2 | C | T | R |
|---|---|---|---|---|---|---|---|
| 2s−4s | −42 | −50 | −61 | 2s−4s | −42 | −57 | −61 |
| $2p_y-4p_y$ | 48 | 45 | 49 | $2p_y-4p_y$ | 48 | 76 | 49 |
| $2p_z-4p_z$ | 77 | 52 | 58 | $2p_z-4p_z$ | 48 | 52 | 49 |
| $2p_x-4p_x$ | 48 | 45 | 49 | $2p_x-4p_x$ | 77 | 50 | 58 |
| $2p_z-3d_{yz}$ | | | 11 | $2p_y-3d_{xy}$ | | | 14 |
| $2p_y-3d_{yz}$ | | 21 | 14 | $2s-3d_{z^2}$ | 25 | 23 | 22 |
| $2p_z-3d_{z^2}$ | | 15 | | $2p_z-3d_{xz}$ | | | 13 |
| $2s-3d_{z^2}$ | 101 | 95 | 89 | $2s-3d_{x^2-y^2}$ | 75 | 72 | 67 |
| $2p_z-3d_{xz}$ | | | 11 | $2p_x-3d_{xz}$ | | 14 | 11 |
| $2p_x-3d_{xz}$ | | 21 | 14 | $2p_x-3d_{xy}$ | | | 11 |

[a] See footnote for Table 5.

**TABLE 9: Ti−O Overlap Populations of $PbTiO_3$[a]**

| Ti−O1 | C | T | R | Ti−O2 | C | T | R |
|---|---|---|---|---|---|---|---|
| 2s−4s | 32 | 37 | | 2s−4s | 32 | 14 | |
| $2p_y-4p_y$ | 29 | 25 | 19 | $2p_y-4p_y$ | 29 | 25 | 19 |
| $2p_z-4p_z$ | 70 | 24 | 47 | $2p_z-4p_z$ | 29 | 25 | 19 |
| $2p_x-4p_x$ | 29 | 25 | 19 | $2p_x-4p_x$ | 69 | 51 | 47 |
| $2p_z-3d_{yz}$ | | | 28 | $2p_x-3d_{xz}$ | | 56 | |
| $2p_y-3d_{yz}$ | | 42 | 30 | $2p_z-3d_{z^2}$ | | 23 | 14 |
| $2p_z-3d_{z^2}$ | | 33 | | $2s-3d_{z^2}$ | 21 | 10 | |
| $2s-3d_{z^2}$ | 84 | 65 | 34 | $2s-3d_{x^2-y^2}$ | 64 | 40 | 25 |
| $2p_z-3d_{xz}$ | | | 30 | $2p_x-3d_{xz}$ | | | 29 |
| $2p_x-3d_{xz}$ | | 42 | 13 | $2p_y-3d_{x^2-y^2}$ | | 18 | 25 |
| $2p_y-3d_{z^2}$ | | | 22 | $2p_x-3d_{xy}$ | | | 29 |
| $2p_x-3d_{z^2}$ | | | 22 | | | | |

[a] See footnote for Table 5.

populations change from negative to positive. However, the $2s-3d_{z^2}$ overlap populations decrease from 105 in $CaTiO_3$ to 84 in $PbTiO_3$. Furthermore, the $2p_y-4p_y$ and $2p_x-4p_x$ overlap populations also decrease with the increase of A atomic number. In lower symmetry T and R structures, new bonding is formed between titanium and oxygen atoms, which leads to enhancement of Ti−O bonding. From the calculated bond orders (Table 4) and overlap populations (Tables 6−9), one can see that enhancement of Ti−O bonding due to symmetry lowering is a common feature of all the $ATiO_3$ compounds, implying elucidation of the different ferroelectric behaviors of perovskites from the point of view of Ti−O interaction only is inconvincible and the A−O interaction should be taken into account. Examining the listed overlap populations, one can conclude that the enhancement of Ti−O bonds in lower symmetry structures (T and R) is mainly due to the interactions between p atomic orbitals (AOs) of oxygen and d AOs of titanium.

## Conclusions

In this paper we have performed a comparative study on the four $ATiO_3$ perovskite compounds based on the experimentally and theoretically optimized lattice structures. The calculated total energies and potential energy surfaces show that it is difficult for $CaTiO_3$ and $SrTiO_3$ to have *P*4*mm* and *R*3*m* ferroelectric structures. The ground-state structures for $BaTiO_3$ and $PbTiO_3$ are rhombohedral and tetragonal structures, respectively. Potential energy surfaces and superlattice calculations show that the eight-site model is favorable in energy. Our calculated potential energy surfaces support the experimental conclusion that Ti displaces from ⟨111⟩ axes to the polarization axis due to tetragonal strain. Electronic structure calculations indicate that from Ca to Ba the A−O covalent bonding becomes weaker. Analyses show that Pb bonds to O mainly with its 6p AOs whereas Ca, Sr, and Ba atoms link to oxygen atoms through the *n*s−2s bonding. Analyses also show that enhancement of Ti−O bonding in lower symmetry structures is mainly due to

interaction between p of oxygen and d of titanium. Charges on A and A−O bond orders show different variation behaviors between ferroelectrics $BaTiO_3$ and $PbTiO_3$ and incipient ferroelectrics $CaTiO_3$ and $SrTiO_3$, indicating that the different ferroelectric behaviors of the $ATiO_3$ perovskites closely relate to charges on A and A−O interaction and more attention should be paid to them.

## References and Notes

(1) Lines, M. E.; Glass, A. M. *Principles and Applications of Ferroelectrics and Related Materials*; Clarendon Press: Oxford, U.K., 1977.
(2) Lemanov, V. V.; Sotnikov, A. V.; Smirnova, E. P.; Weihnacht, M.; Kunze, R. *Solid State Commun*. **1999**, *110*, 611.
(3) Cochran, W. *Adv. Phys.* **1960**, *9*, 387.
(4) Ravel, B.; Stern, E. A.; Vedrinskii, R. I.; Kraizman, V. *Ferroelectrics* **1998**, *206*, 407.
(5) Bersuker, I. B. *Phys. Lett*. **1966**, *20*, 589.
(6) Bersuker, I. B. *Ferroelectrics* **1995**, *164*, 75 and references therein.
(7) Comes, R.; Lambert, M.; Guinier, A. *Solid State Commun*. **1968**, *6*, 715.
(8) Comes, R.; Lambert, M.; Guinier, A. *Acta Crystallogr*. **1970**, *A26*, 244.
(9) Yacoby, Y.; Girshberg, Y.; Stern, E. A. *Z. Phys. B* **1997**, *104*, 725.
(10) Sicron, N.; Ravel, B.; Yacoby, Y.; Stern, E. A.; Dogan, F.; Rehr, J. J. *Phys. B* **1995**, *208 & 209*, 319.
(11) Ravel, B.; Sicron, N.; Yacoby, Y.; Stern, E. A.; Dogan, F.; Rehr, J. J. *Ferroelectrics* **1995**, *164*, 265.
(12) Dougherty, T. P.; Wiederrecht, G. P.; Nelson, K. A. *Ferroelectrics* **1995**, *164*, 253.
(13) Dougherty, T. P.; Wiederrecht, G. P.; Nelson, K. A.; Garrett, M. H.; Jensen, H. P.; Warde, C. *Science* **1992**, *258*, 770.
(14) Müller, K. A.; Berlinger, W. *Phys. Rev. B* **1986**, *34* (9), 6130.
(15) Sokoloff, J. P.; Chase, L. L.; Rytz, D. *Phys. Rev. B* **1988**, *38* (1), 597.
(16) Kwei, G. H.; Billinge, S. J. L.; Cheong, S.-W.; Saxton, J. G. *Ferroelectrics* **1995**, *164*, 57.
(17) Vogt, H. *Phys. Rev. B* **1995**, *51*, 8046.
(18) Bersuker, I. B.; Gorinchoi, N. N.; Fedorco, T. A. *Ferroelectrics* **1994**, *153*, 1. The orbitals of A atoms were not taken into account in this reference. It was claimed, however, that elucidation of role of the $A^{2+}$ was in progress.
(19) Miura, K.; Tanaka, M. *Jpn. J. Appl. Phys.* **1996**, *35*, Part 1 (5A), 2719.
(20) Cohen, R. E. *Nature* **1992**, *358*, 136.
(21) Cohen, R. E.; Krakauer, H. *Ferroelectrics* **1992**, *136*, 65.
(22) Zhong, W. *Physics of Ferroelectric*; Scientific Press: Beijing, 1998.
(23) Milsui, T.; Nomura, S. *Numerical Data and Functional Relationships in Science and Technology*; Landolt-Bornstein III: New York, 1981; Vol. 16.
(24) Kennedy, B. J.; Howard, C. J.; Chakoumakos, B. C. *J. Phys. Condens. Matter* **1999**, *11*, 1479.
(25) Ihm, J.; Zunger, A.; Cohen, M. L. *J. Phys. C* **1979**, *12*, 4409.
(26) Payne, M. C.; Teter, M. P.; Allan, D. C.; Arias, T. A.; Joannopoulos, J. D. *Rev. Mod. Phys*. **1992**, *64*, 1045.
(27) Perdew; J. P.; Wang, Y. *Phys. Rev.* **1992**, *B46*, 6671.
(28) Delley, B. *J. Chem. Phys*. **1990**, *92*, 508.
(29) Delley, B. *J. Chem. Phys.* **1991**, *94*, 7245.
(30) Chen, Z. X.; Chen, Y.; Jiang, Y. S. *J. Phys. Chem. B* **2001**, *105*, 5766.
(31) Chen, Z. X.; Liu, Ch. G.; Chen, Y.; Jiang; Y. S. *Chem. Phys.* **2001**, *270* (2), 253.
(32) Rabe, K. M.; Waghmare, U. V. *Ferroelectrics* **1995**, *164*, 15.
(33) Mayer, I. *Chem. Phys. Lett*. **1983**, *97*, 270.
(34) Hirshfeld, F. L. *Theor. Chim. Acta* **1944**, *44*, 129.
(35) Mayer, I. *Int. J. Quantum Chem*. **1986**, *29*, 73.
(36) Mayer, I. *J. Mol. Struct. (THEOCHEM)* **1989**, *186*, 43.
(37) Somogyi, Á.; Tamás, J. *J. Phys. Chem*. **1990**, *94*, 5554.
(38) Hudson, L. T.; Kurtz, R. L.; Robey, S. W.; Temple, D.; Stockbauer, R. L. *Phys. Rev*. **1993**, *B47*, 1174.
(39) Ghosez, Ph.; Gonze, X.; Lambin, Ph.; Michenaud, J.-P. *Phys. Rev*. **1995**, *B51*, 6765.
(40) Ghosez, Ph.; Gonze, X.; Michenaud, J.-P. *Ferroelectrics* **1995**, *164*, 113.
(41) Nemoshkalenko, V.V.; Timoshevskii, A. *Phys. Stat. Solidi B* **1985**, *127*, 163.